International Journal of Modelling & Simulation, Vol. 13, No. 4, 1993

MODELLING AND MEASUREMENT OF NEAR-SURFACE OCEANIC WINDS

D. G. LONG
Electrical and Computer Engineering Department, Brigham Young University
459 Clyde Building
Provo, Utah 84602 USA

Abstract

High-resolution global measurement of the near-surface wind field over the ocean's surface is of critical importance in weather forecasting and in many oceanographic and meteorological studies. Such measurements can be provided by space-borne radar scatterometers. Scatterometers make indirect measurements of the wind by first measuring the surface radar backscatter from which the wind vector is "retrieved" or estimated. A new model-based technique for wind estimation promises improved measurement accuracy. This method is based on a mesoscale model for the near-surface oceanic wind field. The wind field model represents a trade-off between modelling accuracy and computational complexity in the estimation procedure. It is based on the geostrophic approximation and simplistic assumptions about the wind field vorticity and divergence, but includes ageostrophic winds. Simulation of oceanic wind fields and the scatterometer measurement system played a key role in the development and evaluation of the model. In this paper, the development and evaluation of the wind field model is described. The role of simulation in performing trade-offs between the model accuracy and the computational complexity of the model-based estimation procedure is discussed. The model development is an excellent case study of how modelling can be applied to improve the performance of a complex measurement system, and how simulation can be applied to develop and evaluate modelling techniques. A brief comparison of wind estimates made from simulated measurements and estimates based on actual measurements made by the SEASAT scatterometer is provided.

Key Words
Wind field modelling, model-based estimation, scatterometry

1. Introduction

In the mid 1980s, the NASA-sponsored experimental satellite SEASAT demonstrated, among other things, that winds over the ocean could be measured from space using a wind scatterometer [2, 3, 11]. A scatterometer measures the wind-dependent radar backscatter of the ocean's surface, from which the speed and direction of the wind over the ocean's surface are estimated. Unfortunately, the pointwise estimation procedures traditionally used result in nonunique estimates of the wind vector [6]. Since a single estimate of the wind is required for most oceanographic and meteorological studies, the ambiguity in the wind vector estimate is resolved using an error-prone *dealiasing step* to select a unique wind field map (see also [9] and [13]).

A new model-based estimation procedure ameliorates the difficulties associated with these traditional pointwise wind retrieval techniques and can produce more accurate estimates of the wind field [4, 5]. Key to the success of this method is the model of the near-surface wind field. The model represents a tradeoff between modelling accuracy and computational complexity. In this paper the derivation of the wind field model, and the simulation methodology used to evaluate the modelling accuracy, will be briefly described.

An outline of this paper is as follows: first, background information in wind scatterometry is provided, followed by a brief description of the traditional wind estimation approach. The derivation of the wind field model is then described. The simulation methodology used for the evaluation of the wind field model and for selecting the model order is then considered. Finally, the accuracy of the estimated winds using the model-based and traditional pointwise techniques are compared using simulated and actual SEASAT scatterometer measurements.

2. Background

The normalized radar backscatter (σ^o) (at Ku band) of the ocean's surface depends on the wind speed and the relative azimuth angle between the radar illumination and the wind direction, in a manner which varies with the incidence angle of the radar on the ocean surface and the radar polarization [11]. The relationship between σ^o and the wind is known as the *geophysical model function* and will be denoted by $\mathcal{M}$. A typical example of $\mathcal{M}$ is the SASS-2 model function which relates σ^o to the neutral stability wind at 19.5 m [12] (see also [6]). Figure 1 illustrates the characteristics of the SASS-2 model function. Note the $\cos 2\chi$ dependence of σ^o on the relative azimuth angle χ between the radar illumination and the wind direction.

Since $\mathcal{M}$ has a multivalued inverse, several measurements of σ^o from different azimuth angles must be used in order to make inferences about the wind field. The SEASAT scatterometer (SASS) obtained σ^o measurements from only two azimuth angles on an irregular sampling grid. Future scatterometers such as NSCAT [8] will obtain σ^o measurements from three or more azimuth angles on an equally-spaced grid of sample points over the measurement swath. These noisy measurements of σ^o provide an essentially instantaneous sample of the wind field across the swath over the ocean's surface. The problem is to estimate the original wind field at the sample points from the noisy σ^o measurements.

In the traditional approach, the noisy σ^o measurements are used in a pointwise estimation scheme in which only the σ^o measurements for a given grid cell are used to estimate the wind for that cell. An objective function (typically based on the likelihood function) formulated using the noisy σ^o measurements, is minimized with respect to the wind speed and direction at the sample point. Unfortunately, due to the nature of $\mathcal{M}$, the objective function is minimized by several wind vectors. This approach is unable to uniquely estimate the wind vector and several ambiguous wind estimates result for each cell [6]. To select a single wind estimate for each cell, a post-estimation procedure known in the literature as *dealiasing* or *ambiguity removal* is used [9, 10, 13]. Dealiasing procedures have used various *ad hoc* measures and/or pattern recognition of significant weather features to select a wind vector at each sample point of the wind field.

In model-based estimation, the entire wind field over the measurement swath is estimated. By using a model for the surface wind field, this new approach also provides more accurate wind field estimates by taking advantage of the inherent correlation in the wind between different sample points. To estimate the wind field an objective function is formulated using the noisy σ^o measurements. The objective function is based on maximum likelihood, and model parameters are estimated by minimizing the function. Finally, the estimated wind field is computed from the model parameters.

Crucial to the success of this method is a suitably accurate mathematical model for describing and/or representing the near-surface mesoscale ($\sim$ 50 km resolution) wind field over the ocean. Since other data sources

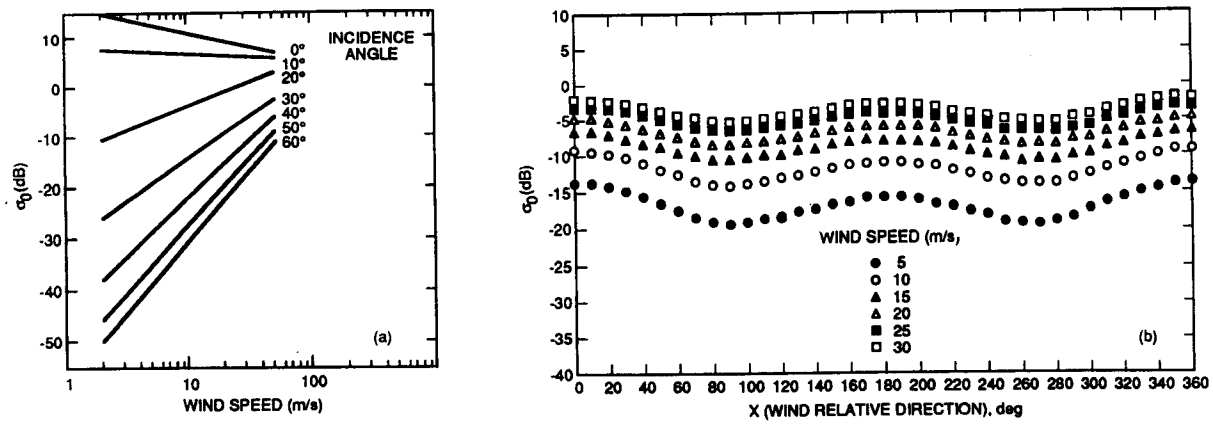

Fig. 1. (a) Incidence angle dependence of the SASS-2 geophysical model function; (b) Relative azimuth angle and wind speed dependence of the SASS-2 geophysical model function.

are not always available, the model must be based on only scatterometer data. To be useful for wind field estimation, the model must be computationally tractable, and lend itself to a model parameter estimation formulation. Note that while the model formulation is based on physical principles, the model does not necessarily have to be based on atmospheric dynamics since the model is used only for describing a snapshot of the near-surface wind field and not for propagating winds.

A particularly simple wind field model which is suitable for wind retrieval can be derived based on the geostrophic equation and rather simplistic assumptions regarding the divergence and curl of the wind field.

3. Development of The Wind Field Model

The wind field model provides a description of the wind field over the scatterometer measurement swath at a fixed instant of time and a resolution of 50 km (corresponding to the SASS spatial sampling). To simplify matters, we restrict our attention to a limited-area swath segment with a maximum spatial extent of approximately 500 km square.

We denote the near-surface horizontal wind field of interest by $\mathbf{U} = (u, v)^T$. We are interested in a mathematical model which will provide a reasonably accurate description of $\mathbf{U}$ over a (limited-area) region $\mathcal{L}$. The vorticity ζ and divergence δ of $\mathbf{U}$ are defined as

$$\zeta = \mathbf{k} \cdot \nabla \times \mathbf{U} \tag{1}$$

$$\delta = \nabla \cdot \mathbf{U} \tag{2}$$

Using the Helmholtz theorem, $\mathbf{U}$ may be defined by a streamfunction ψ and velocity potential χ, according to

$$\mathbf{U} = \mathbf{k} \times \nabla\psi + \nabla\chi \tag{3}$$

where $\mathbf{k} \times \nabla\psi$ is a nondivergent vector field and $\nabla\chi$ is a curl-free vector field (see [7]).

Taking the divergence and curl, respectively, of equation (3), we obtain Poisson equations for ψ and χ:

$$\nabla^2\psi = \zeta \tag{4}$$

$$\nabla^2\chi = \delta \tag{5}$$

These equations appear in the classic problems of partitioning a given wind field into its rotational and non-divergent components and reconstructing a wind field from specified vorticity and divergence [1]. For the latter problem, Lynch [7] argues that the reconstruction is not unique over a limited domain; an arbitrary harmonic function may be added to χ, provided ψ is also altered, to produce the same wind field. From this Lynch concludes that the boundary values of χ may be set arbitrarily. He shows that setting the boundary values of χ to zero minimizes the divergent component of the kinetic energy. Choosing $\chi = 0$ on the boundary ensures a unique reconstruction of the wind field.

Following this line of reasoning, our *first* modelling assumption is that $\chi = 0$ on the region boundary. This corresponds to wind fields with minimum divergent kinetic energy. Assuming that $\chi = 0$ on the boundary, equations (4) and (5), the vorticity and divergence fields, and the boundary conditions for ψ, are sufficient for describing the wind vector field.

To obtain simple boundary conditions we make a *second* major modelling assumption by attributing ψ to the geostrophic motion. This second assumption is that the streamfunction ψ is proportional to the geostrophic pressure field p,

$$\psi = \frac{1}{\rho_s f} p \tag{6}$$

where ρ_s is the density and f is the Coriolus parameter. Note that in a strictly geostrophic formulation, the wind field would be nondivergent and χ would be zero. In the more general formulation which we will adopt, χ corresponds to the *ageostrophic* component of the wind. This generalization allows us to apply the model to mesoscale wind fields which depart from strict geostrophy. Inclusion of the ageostrophic flow permits the model to span a wider space in describing the wind field.

By making this second assumption, the boundary values for equations (4) and (5) can be specified in terms of the geostrophic pressure field. This avoids the difficulties of using velocity boundary conditions which may yield an overdetermined system [7].

Our *third* modelling assumption is that over the region of interest, $\rho_s f$ is essentially constant (i.e., an f-plane approximation); we do this to simplify the mathematics. We can then normalize the pressure field by $\rho_s f$ so that $\psi = p$, i.e., ψ is then the normalized geostrophic pressure field. Then, equation (3) can be written in component form as

$$u = -\frac{\partial p}{\partial y} + \frac{\partial \chi}{\partial x} \tag{7}$$

$$v = \frac{\partial p}{\partial x} + \frac{\partial \chi}{\partial y} \tag{8}$$

These two equations, along with equations (4) and (5), form the basis of the wind field model.

To complete the wind field model, descriptions of the vorticity and divergence fields are needed. Our *fourth* and final assumption is that the vorticity and divergence fields are relatively smooth and can be adequately modeled by low-order bivariate polynomials over the region of interest. Note that the coefficients of the polynomials will be derived from the observed wind fields. For this paper, the following bivariate forms for the vorticity and divergence fields will be assumed:

$$\zeta(x, y) = \sum_{m=0}^{M_C} \sum_{n=0}^{M_C} c_{m,n} x^m y^n \quad \text{for } m + n \leq M_C \tag{9}$$

$$\delta(x, y) = \sum_{m=0}^{M_D} \sum_{n=0}^{M_D} d_{m,n} x^m y^n \quad \text{for } m + n \leq M_C \tag{10}$$

where M_C and M_D are the model orders, and $c_{m,n}$ and $d_{m,n}$ are the model parameters. The number of parameters in the vorticity and divergence field models are $N_C = (M_C+1)(M_C+2)/2$, and $N_D = (M_D+1)(M_D+2)/2$, respectively. Selections of M_C and M_D will be made later based on simulation. Typically, $M_C = M_D = 2$ is adequate for wind estimation.

To solve equations (4), (5) and (7) through (10), these equations are discretized on an $M \times N$ equally-spaced grid with spacing $h = 50$ km over the desired region $\mathcal{L}$ corresponding to the 50 km sampling resolution of SASS. M and N represent selectable model parameters. The swath is also segmented into smaller regions in the along-track dimension (N) to reduce computational requirements. The pressure and velocity potential fields can be eliminated from the discretized system of equations, and the velocity field can be written directly in terms of the pressure-field boundary conditions, and the parameters of the vorticity and divergence fields. The resulting equation relating the velocity-component fields to pressure-field boundary conditions and the vorticity and divergence model parameters can be expressed as

$$\begin{bmatrix} \overline{U} \\ \overline{V} \end{bmatrix} = F\overline{X} \tag{11}$$

where the MN-element vector $\overline{U}$ is the lexicographic-ordered u-component wind field at grid sample points, $\overline{V}$ is the lexicographic-ordered v-component wind field, and the $\overline{X}$ vectors contain $2M + 2N - 2$ pressure-field boundary conditions and $N_C + N_D$ vorticity and divergence field parameters [4]. The full-rank rectangular matrix F consists of known constants. The number of unknowns in the model can be further reduced, at the expense of modelling accuracy, by parameterizing the pressure-field boundary conditions using a periodic polynomial (see [4]).

Equation (11) provides a parametric wind field model which relates the model parameters (in $\overline{X}$) to the wind field (in $\overline{U}$ and $\overline{V}$). This wind field model easily lends itself to the parameter estimation formulation: the model parameters in $\overline{X}$ are directly estimated from the noisy σ^o measurements and the wind field is then computed from the parameters using equation (11). Estimation of $\overline{X}$ from the noisy σ^o measurements is done using the maximum-likelihood (ML) principle: the negative log-likelihood of the model parameters is minimized to estimate the model parameters.

Unfortunately, minimization of the log-likelihood function is computationally intensive. For a fixed swath size, the computation required is inversely proportional to the region area (i.e., $M \times N$) and proportional to a power of the number of unknowns in the model; hence, we desire to minimize the number of unknowns while maximizing M and N. The number of unknowns is a function of the region size (as determined by M and N) and the model orders M_C and M_D. The number of unknowns increases as these parameters increase. However, as shown below, the modelling accuracy *decreases* with increasing M and N, but *increases* for increasing M_C and M_D; hence, selection of the region size and model orders must be made by trading-off modelling accuracy against the computation required to minimize the ML objective function.

4. Wind Field Model Evaluation

To evaluate the capability of the model to accurately describe and model mesoscale winds, we are forced to resort to simulation since there is little conventional oceanic mesoscale data available. Simulated mesoscale test wind fields were generated starting with a state-of-the-art numerical weather prediction model at 1.875 deg resolution (see [10]). These fields were then interpolated to 10 km, and small-scale variability with a ak^{-2} spectrum was added. For a given 2000 × 2000 km region, the value of a was selected to be consistent with the spectrum within the region. The wind fields were selected to span a wide range of meteorological conditions [10]. These fields were used as the "true" wind fields for the evaluation of the wind field model.

To select the vorticity and divergence model order, a grid size (M and N) was chosen and the modelling error evaluated for different model orders M_C and M_D. The modelling error was computed as follows. At a given location, the model parameters $\overline{X}$ were computed, by

$$\hat{\overline{X}} = (F^T F)^{-1} F^T \begin{bmatrix} \overline{U} \\ \overline{V} \end{bmatrix} \tag{12}$$

where $\overline{U}$ is the simulated wind field. The "model" wind field computed from $\hat{\overline{X}}$, is

$$\begin{bmatrix} \widehat{\overline{U}} \\ \widehat{\overline{V}} \end{bmatrix} = F\hat{\overline{X}}. \tag{13}$$

The root mean square (RMS) errors (in vector magnitude, speed, and direction) between the true field and the model field were computed for each segment of the wind field and summed. The results for $M = N = 10$ (a 500×500 km region $\mathcal{L}$) and various M_C and M_D are shown in table 1. $M = 10$ (500 km) was chosen to correspond to the usable SASS swath width. The effects of varying $M = N$ but holding M_C and M_D fixed are illustrated in table 2. Finally, the effects of varying N but holding $M = 10$, $M_C = 2$, and $M_D = 2$ fixed are illustrated in table 3.

Table 1
Wind Field Modelling Error $N = 12$

Model Order		RMS Error		
		Vector Magnitude	Direction	Speed
M_C	M_D	(m/s)	(deg)	(m/s)
N/A†	N/A†	0.299	15.359	0.173
0	0	0.153	7.901	0.089
1	1	0.099	5.444	0.059
2	2	0.086	4.769	0.050
3	3	0.084	4.610	0.049
4	4	0.079	4.391	0.046

† Zero divergence and curl

Table 2
Wind Field Modelling Error M_C=M_D=2

	RMS Error		
	Vector Magnitude	Direction	Speed
$M = N$	(m/s)	(deg)	(m/s)
4	0.033	1.099	0.015
6	0.082	3.489	0.044
8	0.087	4.165	0.048
10	0.086	4.769	0.050
12	0.087	5.354	0.052

Table 3
Wind Field Modelling Error $M = 10$ & M_C=M_D=2

	RMS Error		
	Vector Magnitude	Direction	Speed
N	(m/s)	(deg)	(m/s)
6	0.083	4.071	0.047
8	0.085	4.377	0.049
10	0.086	4.769	0.050
12	0.086	5.058	0.051
14	0.087	5.383	0.053

To summarize, for a fixed M and N, as the model orders are increased, the RMS errors decrease, and the number of unknowns grows. For fixed M_C and M_D, the RMS errors increase as M and N increase though the number of unknowns decreases. Finally, for fixed M, M_C and M_D, the RMS errors increase as N is increased, though relatively slowly. Based on the requirements for scatterometer measurement accuracy (see [4]) and the results of the next section, $M = N = 10$ and $M_C = M_D = 2$ keep the number of unknowns small while providing acceptable model accuracy.

5. System Simulation

The accuracy of the scatterometer-derived wind using the model-based estimation approach is a function not only of the model, but also of the scatterometer σ^o measurement accuracy and the observation geometry (see [6]). Since the RMS errors due to the latter two effects can be large, some modelling error can be tolerated in order to reduce the required computation.

To evaluate the total measurement accuracy, two approaches have been used using simulated SASS measurements and actual SASS measurements. We will first consider the simulation case.

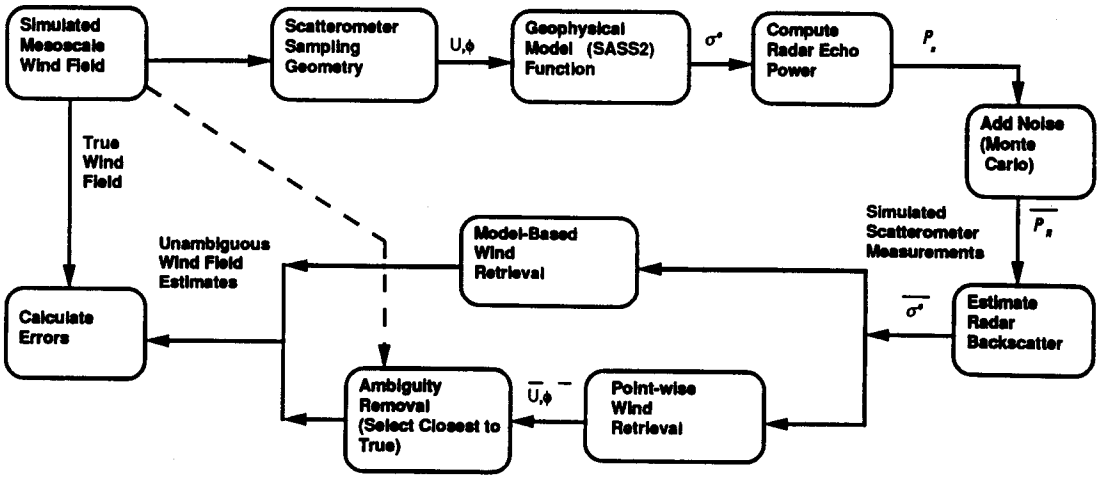

Fig. 2. High-level block diagram of the simulation system (see text).

To make the simulation as accurate as possible, the simulated SASS σ^o measurements were made using the actual SASS observation geometry and sampling. The simulated wind fields described above were used with this geometry and sampling and the SASS-2 model function to compute σ^o. Monte Carlo realization of the system measurement noise was then added.

A noisy measurement z of the true σ^o value may be expressed as

$$z = \sigma^o + \nu \tag{14}$$

where $\nu(k)$ is a zero mean Gaussian random variable whose variance is dependent on the true σ^o. The variance of z (or ν) can be expressed as

$$\mathrm{Var}[z] = \alpha\sigma^{o2} + \beta\sigma^o + \gamma \tag{15}$$

where α, β and γ depend on the observation geometry and the instrument design [11]. The general noise model for the measurements may be expressed as,

$$z = \sigma^o + \nu = \sigma^o[1 + w_1] + \sqrt{\sigma^o}w_2 + w_3 \tag{16}$$

where w_1, w_2 and w_3 are independent, zero mean Gaussian random variables with known variances α, β and γ, respectively. A more detailed description of the system noise model is given in [6]. Values of the parameters α, β and γ were determined from the actual SASS data.

Using the simulated measurements, the wind was estimated using traditional pointwise and model-based estimation. In the case of pointwise estimation, that wind estimate which was closest to the true wind was selected from among the nonunique results as the estimate; thus, the pointwise results will be overly optimistic since there will be errors in selecting the closest estimate when the true wind vector is not known. For model-based estimation, the regions were overlapped 50% in the along-track direction, and were 500 km wide ($M = 10$). The parameters of the wind field model were estimated separately for each region, and the resulting wind field estimates averaged to obtain the wind field over the swath. The RMS error between the true and estimated wind fields were then computed for various model orders and region sizes, and averaged over various noise realizations and swath observation geometries. This can be repeated for each value of N, M, M_C and M_D. Figure 2 shows a high-level block diagram of the simulation/analysis system. While it is impractical to present all results here, table 4 illustrates the RMS errors for both estimation algorithms for the particular case with the model size $M = N = 10$, and the model orders $M_C = M_D = 2$. The error statistics were computed separately in wind-speed ranges as indicated.

Some key observations summarizing the results include: (1) the pointwise wind field estimates have many missing data points (see, for example, fig. 3) since it is not possible to estimate the wind when there are missing σ^o measurements at a given point due the frequent occurrence of instrument calibration cycles (which prevent making a σ^o measurement at the point as the spacecraft passes over); and (2) region sizes of $M = 10$ and $8 \le N \le 14$, with $M_C = M_D = 2$, produce acceptably accurate estimates of the wind with minimum computation. Regarding this latter point, comparison of the model-based and pointwise wind field estimates using simulated data reveals that the model-based wind field estimates (1) appear less "noisy," (2) generally exhibit smaller RMS direction error than the closest pointwise ambiguity (and therefore, from the result of any dealiasing algorithm), and (3) have no missing measurements. The RMS wind speed and RMS vector magnitude error may be slightly larger for the model-based estimates.

Table 4
RMS Difference Between the Estimated and True Fields

Wind Speed Range (m/s)	2-4	4-8	8-12	12-20	20+	All
Model-based						
Number of Wind Vectors	606	2148	2010	1409	300	6473
rms Speed Err (m/s)	0.41	0.42	0.55	0.71	0.88	0.55
rms Direction Err (dir)	11.4	6.7	5.0	3.9	3.6	5.2
rms Vector Mag. Err (m/s)	0.74	0.80	1.01	1.24	1.61	0.96
Pointwise						
Number of Wind Vectors	466	1589	1504	1104	238	4901
rms Speed Err (m/s)	0.42	0.41	0.31	0.29	0.30	0.32
rms Direction Err (dir)	15.4	8.5	4.9	3.8	4.0	7.6
rms Vector Mag. Err (m/s)	0.90	0.84	0.87	1.03	1.56	0.81

Note: Simulated σ^o measurements are used with $M = N = 10$ and $M_C = M_D = 2$. The error statistics were separately computed for each wind speed band.

6. Actual Performance

When using actual SASS measurements, the performance of the model-based estimate is difficult to independently establish since the ground truth wind field is not known. In order to evaluate the performance of the model-based estimates, pointwise dealiased SASS winds must be used. For this purpose the data set generated by Wurtele *et al.* [13] has been used. The Wurtele data set consists of two weeks of manually dealiased SASS winds. The data set is based on winds retrieved on a 100 km grid. Since the model-based wind estimates are at 50 km resolution, a comparison data set has been generated by using pointwise estimation of the SASS winds on a 50 km grid, then selecting the ambiguity which is closest to the corresponding Wurtele unique wind direction.

Figure 3 provides an illustration of this 50 km dealiased wind field for a portion of SEASAT rev 1070 (Sept. 9, 1978). The corresponding model-based estimate is given in figure 4 with $M = 10$, $N = 14$ and $M_C = M_D = 2$. Comparison of the model-based and pointwise wind field estimates reveals that the model-based wind field estimate (1) appears to be less "noisy," (2) has significantly fewer missing wind measurements, and (3) covers a wider, uniform-width swath. Since the actual, underlying wind field is not known, it is difficult to be quantitative in evaluating the measurement accuracy. However, careful comparison of the estimates using both techniques has revealed a few regions where the methods differ significantly. In every case examined thus far, these differences could be attributed to errors in the dealiased results.

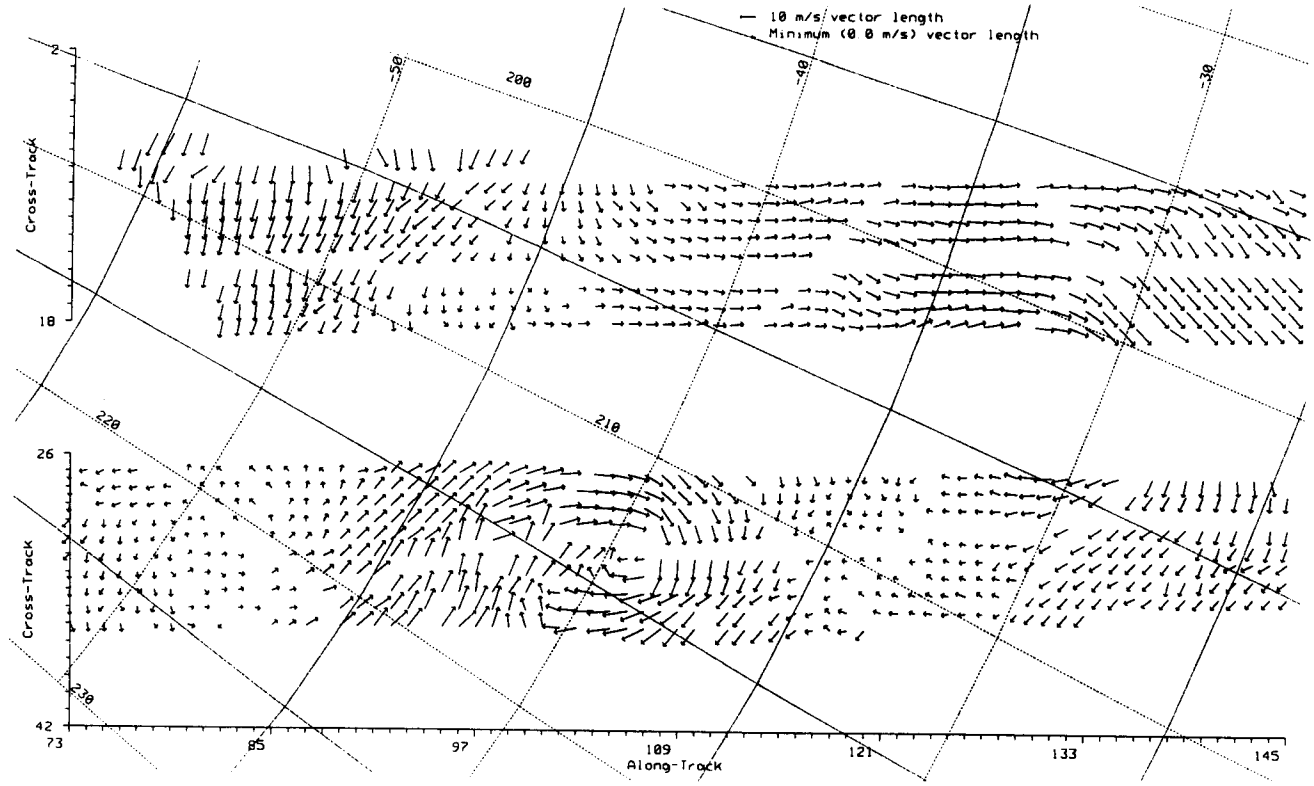

Fig. 3. 50 km resolution dealiased pointwise wind estimate from actual SASS measurements (Rev 1070, Sept. 9, 1978) on a 50 km along-track/cross-track grid. The selected wind direction is based on the 100 km Wurtele [13] data set. Missing σ^o measurements result prevent pointwise wind retrieval at various grid points. Note the use of a minimum vector length to assist in viewing the wind direction at low wind speeds.

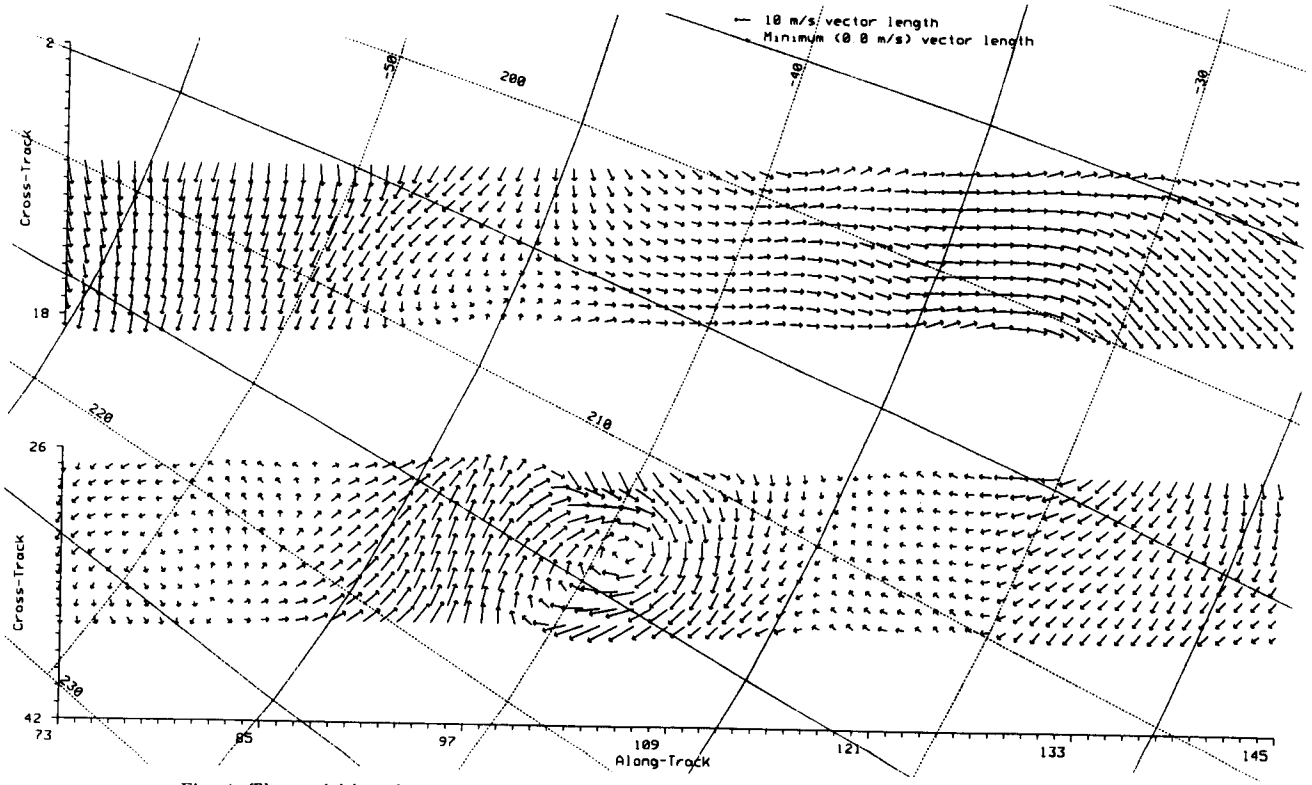

Fig. 4. The model-based estimate corresponding to figure 3. Note the wider, uniform swath width without missing measurements.

Thus, model-based estimation can also provide an accuracy check for more traditionally-derived results. We note that while the Wurtele result is based on many man-hours of expert dealiasing, model-based wind estimation is inherently automated and therefore better suited for future operational scatterometers.

7. Summary

The traditional approach to solving the wind estimation problem leads to multiple solutions requiring *ad hoc* dealiasing techniques to produce a unique solution. The model-based estimation technique, by imposing a model on the underlying wind field, eliminates this error-prone dealiasing step and yields more accurate estimates of the wind *even when perfect dealiasing is assumed.* The improved performance can be attributed to the fact that the model-based approach takes advantage of the inherent correlation between the wind at different sample points to reduce the noise in the final wind estimates. Because of this, the model-based approach is more tolerant of noise in the σ^o measurements than is the pointwise wind estimate technique; the accuracy of the wind fields estimated using a model-based approach degrade gracefully as the SNR of the measurements is reduced. This may permit reductions in the size and weight of future scatterometer instruments by reducing the requirements on the SNR of the σ^o measurements, permitting smaller transmitters, antennas, etc.

Compared to the previously used wind retrieval/dealiasing algorithms, model-based wind retrieval (1) generally produces more accurate directional estimates of the wind, (2) uses more of the available σ^o measurements, including points at which only a single σ^o measurement is available, (3) has fewer "holes" in the estimated wind field, (4) produces a wider measurement swath for SASS, and (5) is less sensitive to the noise level in the σ^o measurements. These results validate the utility of model-based wind estimation.

The methodology used in this research has applications in other areas involving distributed parameter systems. In wind estimation we started with a well-defined measurement equation for a parameter (σ^o) which is related to the quantity of interest (the wind) via a model function. Our approach to the estimation of the wind from measurements of σ^o is to view the wind field as a distributed parameter system which can be approximately modeled using partial differential equations. In effect, this system of equations provides constraints on the estimate of the quantity of interest, thus permitting more accurate estimates.

The partial differential equation system is solved by converting it to a finite-difference system which is then arranged to express the quantity of interest in terms of a set of unknown parameters. This yields a simple model of the distributed parameter system with selectable order. Simulation was then used to select the model order. The desired quantity is estimated indirectly by first estimating the unknown parameters of the model directly from the measurements, then using the model to compute the quantity of interest from the estimated model parameters.

As the results of this research indicate, this methodology can be successfully used even when the relationship between the measured parameter and the desired quantity is non-unique as is the case with the geophysical model function relating σ^o and winds.

Acknowledgements

I am pleased to acknowledge the support of the NASA HQ Physical Oceanography program under Gary Lagerloef and David Adamec. Portions of this research were conducted at the Jet Propulsion Laboratory, California Institute of Technology and at Brigham Young University under NASA contract. Dr. Michael Frelich of JPL supplied the simulated wind fields.

References

[1] S.J. Bijlsma, L.M. Hafkenscheid & P. Lynch, "Computation of the Streamfunction and Velocity Potential and Reconstruction of the Wind Field." *Monthly Weather Review*, **114**, 1986, 1547-1551.

[2] M.H. Freilich, "Satellite Scatterometer Comparisons with Surface Measurements: Techniques and SEASAT Results." *Proc. of a Workshop on ERS-1 Wind and Wave Calibration*, (June 2-6, 1986), *ESA SP-262*, September 1986, 57-62.

[3] W.L. Jones, L.C. Schroeder, D.H. Boggs, E.M. Bracalente, R.A. Brown, G.J. Dame, W.J. Pierson & F.J. Wentz, "The SEASAT-A Satellite Scatterometer: The Geophysical Evaluation of Remotely Sensed Wind Vectors Over the Ocean" *J. of Geophysical Research*, **87**(C5), 3297-3317.

[4] D.G. Long & J.M. Mendel, "Model-Based Estimation of Wind Fields Over the Ocean from Wind Scatterometer Measurements I: Development of the Wind Field Model." *IEEE Trans. on Geoscience and Remote Sensing*, **28**(3), 349-360.

[5] D.G. Long & J.M. Mendel, "Model-Based Estimation of Wind Fields Over the Ocean from Wind Scatterometer Measurements II: Model Parameter Estimation." *IEEE Trans. on Geoscience and Remote Sensing*, **28**(3), 361-373.

[6] D.G. Long & J.M. Mendel, "Identifiability in Wind Estimation from Wind Scatterometer Measurements." *IEEE Trans. on Geoscience and Remote Sensing*, **29**(2), pp. 268-276.

[7] P. Lynch, "Deducing the Wind from Vorticity and Divergence." *Monthly Weather Review*, **116**, 1988, 86-93.

[8] F. Naderi, M.H. Freilich & D.G. Long, "Spaceborne Radar Measurement of Wind Velocity Over the Ocean–An Overview of the NSCAT Scatterometer System." *Proc. of the IEEE*, **79**(6), 850-866.

[9] L. Schroeder *et al.*, "Removal of Ambiguous Wind Directions for a Ku-band Wind Scatterometer Using Measurements at Three Different Azimuth Angles." *IEEE Transactions on Geoscience and Remote Sensing*, **GE-23**(2), 91-100.

[10] S.J. Shaffer, R.S. Dunbar, S.V. Hsiao & D.G. Long, "A Median-Filter-Based Ambiguity Removal Algorithm for NSCAT." *IEEE Trans. on Geoscience and Remote Sensing*, **29**(1), 167-174.

[11] F.T. Ulaby, R.K. Moore & A.K. Fung, *Microwave Remote Sensing - Active and Passive.* Reading, Mass.: Addison-Wesley Pub. Co., , 1981.

[12] F. J. Wentz, S. Peteherych & L.A. Thomas, "A Model Function for Ocean Radar Cross-sections at 14.6 GHz." *Journal of Geophysical Research*, **89**, 1984, 3689-3704.

[13] M.G. Wurtele *et al.*, "Wind Direction Alias Removal Studies of SEASAT Scattermeter-Derived Wind Fields." *J. of Geophysical Research*, **87**(C5), 3365-3377.